

Nonlocal Detection of Interlayer Three-Magnon Coupling

Lutong Sheng^{1,*}, Mehrdad Elyasi^{2,*}, Jilei Chen^{3,4,*}, Wenqing He^{5,*}, Yizhan Wang⁵, Hanchen Wang^{1,4}, Hongmei Feng⁶, Yu Zhang⁵, Israa Medlej^{3,4}, Song Liu^{3,4}, Wanjun Jiang⁶, Xiufeng Han⁵, Dapeng Yu^{3,4}

Jean-Philippe Ansermet^{7,3}, Gerrit E. W. Bauer^{2,8,9,10} and Haiming Yu^{1,4,†}

¹*Fert Beijing Institute, MIIT Key Laboratory of Spintronics, School of Integrated Circuit Science and Engineering, Beihang University, Beijing 100191, China*

²*WPI Advanced Institute for Materials Research, Tohoku University, Sendai 980-8577, Japan*

³*Shenzhen Institute for Quantum Science and Engineering,*

Southern University of Science and Technology, Shenzhen 518055, China

⁴*International Quantum Academy, Shenzhen 518048, China*

⁵*Beijing National Laboratory for Condensed Matter Physics, Institute of Physics, University of Chinese Academy of Sciences, Chinese Academy of Sciences, Beijing 100190, China*


⁶*State Key Laboratory of Low-Dimensional Quantum Physics and Department of Physics, Tsinghua University, Beijing 100084, China*

⁷*Institute of Physics, Ecole Polytechnique Fédérale de Lausanne (EPFL), 1015, Lausanne, Switzerland*

⁸*Institute for Materials Research, Tohoku University, Sendai 980-8577, Japan*

⁹*Center for Spintronics Research Network, Tohoku University, Sendai 980-8577, Japan*

¹⁰*Zernike Institute for Advanced Materials, University of Groningen, 9747 AG Groningen, Netherlands*

 (Received 7 September 2022; revised 9 November 2022; accepted 21 December 2022; published 24 January 2023)

A leading nonlinear effect in magnonics is the interaction that splits a high-frequency magnon into two low-frequency magnons with conserved linear momentum. Here, we report experimental observation of nonlocal three-magnon scattering between spatially separated magnetic systems, viz. a CoFeB nanowire and a yttrium iron garnet (YIG) thin film. Above a certain threshold power of an applied microwave field, a CoFeB Kittel magnon splits into a pair of counterpropagating YIG magnons that induce voltage signals in Pt electrodes on each side, in excellent agreement with model calculations based on the interlayer dipolar interaction. The excited YIG magnon pairs reside mainly in the first excited ($n = 1$) perpendicular standing spin-wave mode. With increasing power, the $n = 1$ magnons successively scatter into nodeless ($n = 0$) magnons through a four-magnon process. Our results demonstrate nonlocal detection of two separately propagating magnons emerging from one common source that may enable quantum entanglement between distant magnons for quantum information applications.

DOI: [10.1103/PhysRevLett.130.046701](https://doi.org/10.1103/PhysRevLett.130.046701)

Nonlinear effects are ubiquitous in a variety of physical systems, such as lasers [1], electron beams [2], cold atoms [3], and water waves [4]. Magnons are the quanta of spin waves, the collective excitations of the magnetic order. In magnon spintronics or magnonics [5–9] they are employed as information carriers for low-power processing and transmission [10–12]. Nonlinearities in the magnetization dynamics have been known for many decades [13–23]. New nonlinear phenomena have been discovered in magnetic textures [24–28], nanoscale magnets [29–31], and hybrid systems [32,33]. Nonlinearity provides rich physics [34] and is relevant for technological applications [35], such as mechanical force sensors [36]. Optical nonlinearities enable the coupling of LC resonators with a superconducting qubit [37]. A nonlinear magnetostrictive interaction may generate magnon-photon-phonon entanglement in cavity magnetomechanics [38]. Nonlinearities generate magnon interaction that leads to “squeezing” of magnon amplitudes [39] and continuous variable quantum

entanglement [40]. The latter is distillable [41] only when nonlocal and quantum entangled over a distance. Separation of entangled magnons appears to be a formidable task, but could be useful in information technologies such as quantum key distribution [42] and quantum teleportation [43].

One leading nonlinear effect in magnetic systems is the three-magnon interaction [18–26], in which a magnon with energy $\hbar\omega$ and zero momentum (Kittel mode) decays into two lower energy (frequency) magnons $\hbar\omega/2$ with opposite wave vectors ($\hbar k$ and $-\hbar k$). It has been observed in yttrium iron garnet (YIG) films [18–21], spin-valve nanocontacts [22], and magnetic vortices [24,25]. In all studies, the three magnons are part of the same magnet. Indeed, the magnon interactions are usually assumed to be short-ranged. However, this is not self-evident, since the long-range dipolar interaction contributes too. An interaction between different material systems, e.g., a magnon of system A that decays into two magnons in system B, would offer additional functionality for hybrid [44] and 3D

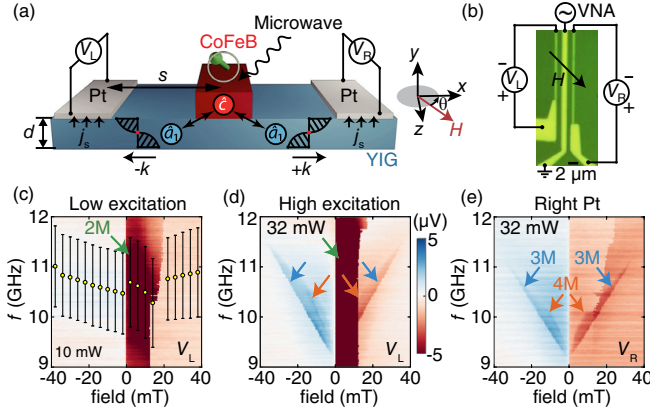


FIG. 1. (a) Schematic (side view) of spin pumping by a CoFeB nanowire detected nonlocally by two Pt electrodes on the left (V_L) and right (V_R) sides. Magnetic field H is applied in the xz plane with an angle $\theta = 45^\circ$ with respect to x . s denotes the distance between the CoFeB wire and a Pt bar. (b) Optical microscopic image of the three-terminal device. The center line is a CoFeB nanowire covered by a gold stripline antenna. Pt electrodes on both sides detect nonlocal spin pumping from the CoFeB wire. (c) V_L measured with field swept from negative to positive values. At an input microwave power of 10 mW, we are still in the linear regime. Green arrow marks the spin pumping induced by the linear magnon-magnon (2M) coupling when the magnetizations are antiparallel. Yellow dots mark the CoFeB resonance frequencies with error bars representing the ferromagnetic resonance (FMR) linewidth. (d) V_L measured at a high input power of 32 mW. The field sweep is the same as in (c). Light blue arrows indicate a mode associated with the interlayer three-magnon (3M) coupling. We attribute another mode (orange arrows) to a secondary nonlinear four-magnon (4M) process. (e) V_R measured at the same condition with (d) for comparison.

magnonics [45]. Here, we demonstrate interlayer three-magnon interactions in a CoFeB|YIG hybrid nanostructure, in which a magnon in a CoFeB nanowire splits into two counterpropagating magnons in a YIG thin film, that are then detected nonlocally at two separated Pt electrodes placed on each side.

We excite the magnetic system that consists of a CoFeB nanowire (200 nm wide, 30 nm thick, and 100 μm long) on top of a YIG film with a thickness $d = 80$ nm [see Fig. 1(a)] by a stripline antenna [46] (1.3 μm wide, 0.1 μm thick, and 100 μm long). The width of CoFeB wire is characterized by the scanning electron microscope (SEM) shown in the Supplemental Material (SM), Sec. I [47]. The

YIG films are deposited on gadolinium gallium garnet substrates by radio-frequency magnetron sputtering. We detect propagating magnons by their spin pumping [53–57] into Pt contacts placed on each side of CoFeB at a distance $s = 2.5$ μm , in which the inverse spin Hall effect (ISHE) generates a transverse voltage. Figure 1(b) is a microscopic image of the device. A magnetic field applied at an angle $\theta = 45^\circ$ [55] with respect to x allows both efficient excitation of the nanowire (maximal for 90°) and detection by ISHE (best for 0°). Moreover, this configuration at 45° is also optimal for the first-order Suhl instability [13,58]. Figure 1(c) shows the ISHE voltage at the left Pt electrode (V_L) as a function of excitation frequency and applied field for a small microwave power of 10 mW, which is safely in the linear regime. The red (blue) color represents negative (positive) voltage response. The relatively strong negative ISHE voltage (~ -6 μV , marked by the green arrow) corresponds to the antiparallel magnetization of the CoFeB and YIG layers with large interlayer magnon-magnon (2M) coupling [59]. The yellow dots denote the CoFeB resonance frequencies extracted from the reflection spectra S_{11} in SM Fig. S2(b) [47] measured by the vector network analyzer (VNA). Figure 1(d) shows V_L under high excitation (microwave power 32 mW). The strong intensity area corresponds to the linear magnon-magnon coupling at the antiparallel configuration of CoFeB|YIG with its nonsaturated color map shown in SM Fig. S3 [47]. We observe additional modes indicated by blue and orange arrows in Fig. 1(d). We argue below that an interlayer three-magnon (3M) process causes the former ones [blue arrows in Fig. 1(d)] and attribute them to parametric pumping of the first excited perpendicular standing spin waves (PSSWs) in YIG by the stray field of the CoFeB Kittel mode [blue arrows in Fig. 2(a)]. The latter one [orange arrows in Fig. 1(d)] should originate from an intralayer four-magnon (4M) scattering [31,60,61] [orange dashed arrows in Fig. 2(a)] following the interlayer three-magnon process (blue arrows). The comparison of V_L in Fig. 1(d) with V_R in Fig. 1(e) confirms the strong chirality of the linear-response modes [62,63] (areas marked by green arrows), while the nonlinear signals (blue and orange arrows) are nearly equally strong for V_L and V_R .

Figure 2(a) shows the dispersion of the nodeless ($n = 0$) and single-node ($n = 1$) perpendicular standing spin waves. The frequency of a spin wave with momentum k in mode n reads [64,65]

$$f_n(k) = \frac{\mu_0\gamma}{2\pi} \sqrt{\left[H_0 + M_s\Lambda_{\text{ex}}k^2 + M_s\Lambda_{\text{ex}}\left(\frac{n\pi}{d}\right)^2 \right] \left[H_0 + M_s\Lambda_{\text{ex}}k^2 + M_s\Lambda_{\text{ex}}\left(\frac{n\pi}{d}\right)^2 + F_nM_s \right]}. \quad (1)$$

In calculations, we use the YIG exchange constant $\Lambda_{\text{ex}} = 3 \times 10^{-16}$ m^2 , saturation magnetization $M_s = 140$ kA/m [66], and film thickness $d = 80$ nm. F_n is the dipolar array factor [67]. For the $n = 1$ mode at

$\theta = 45^\circ$ with $kd \ll 1$, one can derive $F_n \approx 1$ (see SM, Sec. IV [47]). According to our modeling explained below, the CoFeB Kittel mode at ~ 10 GHz couples primarily with the high- k single-node mode as indicated by the green

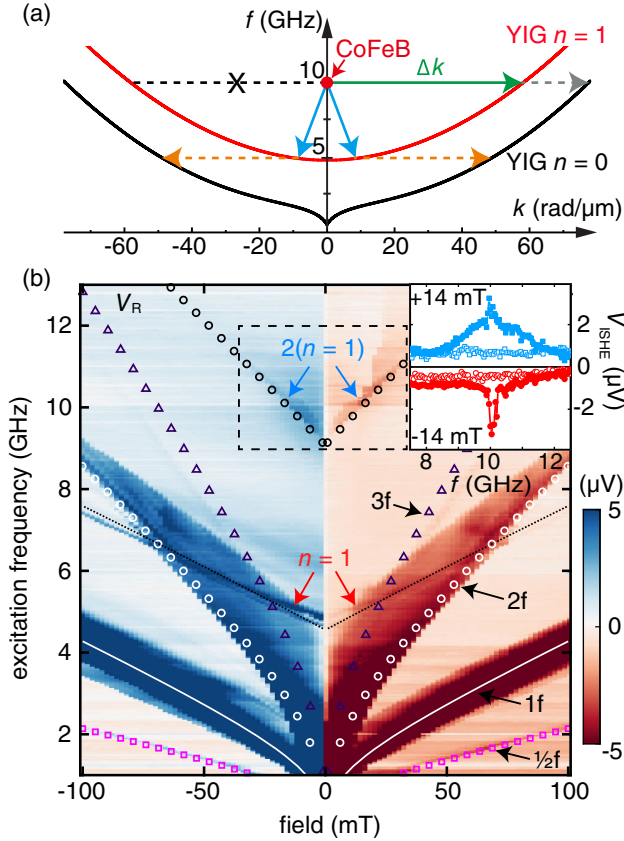


FIG. 2. (a) Spin-wave dispersion of the nodeless ($n = 0$ black curve) and single-node ($n = 1$ red curve) modes for a YIG film with thickness $d = 80$ nm and applied field of 10 mT at $\theta = 45^\circ$. Spin pumping induced by the interlayer two-magnon scattering (green arrow) is unidirectional, while spin pumping by the interlayer three-magnon scattering (blue arrows) is not. Dashed orange arrows: interband secondary four-magnon scattering from the $n = 1$ to $n = 0$ mode. (b) V_R measured at an input power of 32 mW. Black arrows denote excitations of $n = 0$ modes at frequencies $\frac{1}{2}f$ (magenta open squares), f (white solid lines), $2f$ (white circles), and $3f$ (violet open triangles). Red arrows indicate direct excitation of the $n = 1$ modes (black dotted line), while blue arrows indicate their parametric pumping (black circles). The field is swept from negative to positive values. Blue (red) line plot in the inset presents the frequency-dependent ISHE voltage 14 mT (−14 mT). Blue open squares (red circles) are data measured on a bare YIG film without CoFeB wire.

arrow in Fig. 2(a). This linear interlayer magnon coupling is strongly enhanced in the antiparallel configuration, here in the field interval 0–20 mT [59,63]. The linear process by this “two-magnon” scattering is strongly unidirectional due to the interlayer dipolar interaction [62,63], with voltage signals in the left Pt electrode V_L [green arrow in Fig. 1(d)] but not in the right one V_R [Fig. 2(b)]. In this process, the nanometric width of CoFeB wire generates a broad k distribution and thus enables efficient scattering between a $k = 0$ CoFeB magnon and a high- k $n = 1$ YIG magnon given by the dispersion in Fig. 2(a). In the studied system,

the magnon-magnon coupling is mainly contributed by the dynamic dipolar interaction [59,68,69] dominating the interlayer exchange interaction (see SM Fig. S5 [47] for results on control samples with a MgO spacer). The latter plays a more important role in extended bilayer films [70–72]. We derive the interlayer magnon-magnon coupling strength by the magnetodipolar interaction for the $n = 0$ and $n = 1$ modes with $+k$ and $-k$ wave vectors in the SM, Sec. VI-C [47]. The chiral spin pumping signal scales linearly with the microwave power and can be detected down to 1 mW (see SM, Sec. VII [47]). At powers above 10 mW, nonlinear effects emerge. Figure 2(b) shows the spin pumping signals measured on the right Pt electrode at 32 mW with microwave excitation frequencies set from 1 to 13 GHz. The Pt bar serves as a broadband detector. We observe multiple new features associated with the $n = 0$ mode ($1f$) including parametric pumping at $2f$ microwave excitation [54] (calculated as white circles) and $3f$ (calculated as violet open triangles) as well as $\frac{1}{2}f$ (calculated as magenta open squares) comb excitations [22,28]. The $n = 1$ PSSW mode is observed in Fig. 2(b) indicated by the red arrows and calculated as the black dotted line. By varying the YIG film thickness from 80 to 40 nm, the $n = 1$ mode shifts to ~ 12 GHz as shown in the SM, Sec. VIII [47]. Evidence for parametric pumping of the higher $n = 1$ mode appears at high frequencies around 10 GHz as marked by blue arrows and calculated as black open circles. The interaction coefficient of the intermagnet three-magnon scattering is proportional to the square of the YIG magnon mode amplitudes normal to the film and therefore depends only weakly on the mode number n . Figure 1(e) presents an enlarged measurement in the dashed square region with finer field sweeping steps. The inset of Fig. 2(b) shows two line plots at +14 mT (blue squares) and −14 mT (red dots) with positive and negative ISHE voltage signals. Open blue squares and open red circles show data obtained from a bare YIG sample without CoFeB wire on top (see SM, Sec. IX [47]). If we replace the 200-nm-wide CoFeB wire by a 800-nm-wide one, the CoFeB Kittel mode frequency drops significantly and no longer matches twice the frequency of the $n = 1$ mode. As a result, no signal is observed around 10 GHz (see SM, Sec. X [47]). The signals in Fig. 2(b) marked by blue arrows are therefore caused by parametric pumping of $n = 1$ YIG magnons by the stray field from the CoFeB dynamics but not the stripline. In general, one may replace CoFeB by other materials such as CoFe possessing large saturation magnetization [73] and low magnetic damping [74,75] to enhance the interlayer three-magnon coupling efficiency.

Our experiments uniquely combine the advantages of microwave and electrical magnon transport studies. The observable is $S_{21}(\omega_1, \omega_2)$, the bichromatic scattering matrix of a magnon injected at frequency ω_1 at contact or stripline 1 to a magnon with frequency ω_2 at contact or stripline 2.

Propagating magnon spectroscopy [7] studies the coherent magnons at frequency ω in terms of $S_{21}(\omega, \omega)$. Electrical injection and detection of magnons by heavy metal contacts [8] is the method of choice to study diffuse magnon transport. However, this method senses only $\int |S_{21}(\omega_1, \omega_2)| d\omega_1 d\omega_2$, so all spectral information is lost. Here we measure the coherent response to inductive magnon injection at frequency ω and electrical detection at a distant contact, i.e., $\int |S_{21}(\omega, \omega_2)| d\omega_2$. In the linear regime this does not provide new information. However, the emergence of a magnon frequency comb leads to an increased signal at a magnon resonance $\omega = \omega_k$, while new signals due to parametric pumping emerge when $\omega = 2\omega_k$. When the magnon decay length is larger than the contact distance, we can interpret the experiments simply in terms of the magnon spectrum generated by the microwaves under the stripline since the electrical detection is not sensitive to the propagation phase. Here we model the observed nonlinearities by the leading terms in the Holstein-Primakoff expansion with Hamiltonian

$$\hat{\mathcal{H}} = \hat{\mathcal{H}}_C^{(0)} + \hat{\mathcal{H}}_Y^{(0)} + \hat{\mathcal{H}}_{CY}^{3M}, \quad (2)$$

Here $\hat{\mathcal{H}}_C^{(0)} = \varepsilon_C c^\dagger c$ and $\hat{\mathcal{H}}_Y^{(0)} = \sum_{n,\mathbf{k}} \varepsilon_{n,\mathbf{k}} a_{n,\mathbf{k}}^\dagger a_{n,\mathbf{k}}$ are the excitations of the Kittel mode in the magnetic wire and spin waves in mode n , \mathbf{k} of the film. \hat{c} ($\hat{a}_{n,\mathbf{k}}$) is the annihilation operator of the CoFeB nanowire Kittel magnon (YIG magnon of $n = 0, 1$ with wave vector $\mathbf{k} = \vec{k}^\pm$). In principle, all states may be excited by the microwaves emitted by the stripline with mode-dependent efficiencies. The leading nonlinear term is the three-magnon interaction $\hat{\mathcal{H}}_{CY}^{3M}$. In the following, we model the nonlinear excitations observed around the CoFeB resonance frequency (10 GHz) by the magnetodipolar field of the nanowire in the YIG thin film with an interlayer three-magnon interaction $\hat{\mathcal{H}}_{CY}^{(3M)} = \mathcal{D}_{\vec{k}^+ \vec{k}^-}^{(n)} \hat{c}^\dagger \hat{a}_{n,\vec{k}^+} \hat{a}_{n,\vec{k}^-} + \text{H.c.}$, where $\mathcal{D}_{\vec{k}^+ \vec{k}^-}^{(n)}$ is a coefficient, and $\vec{k}^+ \approx -\vec{k}^-$ (see SM, Sec. VI-D [47]). The efficiency of the parametric excitation scales with the ellipticity of the excited magnon pairs, which decreases with k , so $|\mathcal{D}_{\vec{k}^+ \vec{k}^-}^{(1)}| > |\mathcal{D}_{\vec{k}^+ \vec{k}^-}^{(0)}|$. Therefore, the CoFeB Kittel mode excites $n = 1$ YIG magnon pairs at a lower threshold than that of $n = 0$ pairs. The parallel magnetic pumping by the Zeeman interaction ($\mu_0 \gamma \vec{m}_Y \cdot \vec{h}_{\text{dip}}$) does not depend on the polarization of either the magnon nor the dipolar field, in contrast to the chiral spin pumping [62,63]. The three-magnon interaction is therefore not chiral and the signals in both Pt contacts are nearly the same [Figs. 2(b) and 2(c)].

In Fig. 3 we address the power dependence of the signals at 5 and 10 GHz. We focus on the V_{ISHE} on the right Pt electrode for input powers from 1 to 47 mW (see SM, Sec. XI [47]). The signal attributed to the interlayer three-magnon interaction at microwave powers above 20 mW (light green area in Fig. 3) is nearly the same in both

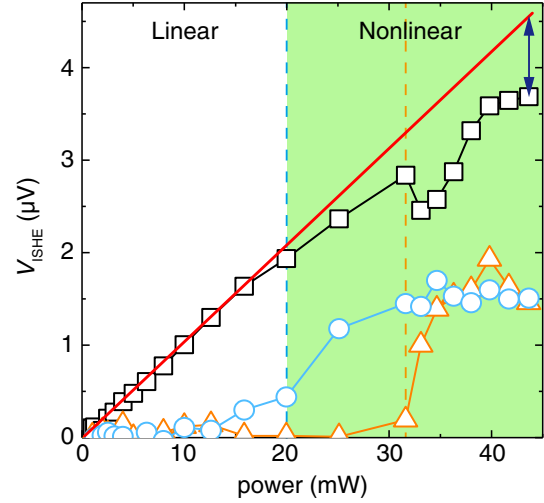


FIG. 3. ISHE peak voltages of the right Pt electrode as a function of the input microwave power measured at 5 GHz for the low- k $n = 1$ PSSW mode (black open squares) and at 10 GHz for the nonlinear modes (light blue open circles and orange open triangles). The red line is a linear fit up to 20 mW. The dark blue double-sided arrow marks the deviation from linearity. The light green area represents the nonlinear regime of interlayer three-magnon processes (light blue open circles) above 20 mW (blue dashed line). An additional feature [orange arrows in Fig. 1(c) and orange open triangles] observed above 32 mW (orange dashed line) is attributed to a secondary four-magnon process as indicated by orange dashed arrows in Fig. 2(a).

contacts. The signal associated to the excitation of the low- k $n = 1$ mode deviates from a linear power dependence (black open squares) at ~ 20 mW, which we interpret as an evidence for the Suhl instability [13]. The spin pumping signal drops above the threshold, because the confluence scattering opposes the Kittel magnon decay in the wire. When the power reaches 32 mW, an additional mode [orange arrows in Fig. 1(d)] emerges. We attribute this additional mode to a four-magnon process [31,60] during which two $n = 1$ YIG magnons scatter to two $n = 0$ YIG magnons, i.e., $a_1^\dagger a_1^\dagger a_0 a_0 + \text{H.c.}$ [orange dashed arrows in Fig. 2(a)]. The drop in the $n = 1$ mode intensity (black open squares) accompanies a new signal (orange open triangles), similar to a four-magnon scattering signal reported for a YIG nanoconduit [31]. We explain the increased slope of the orange mode as a function of field as follows; see also SM, Sec. VI-E [47]. The four-magnon interaction scales like $\propto |\vec{k}^{\prime\pm}|^2$, where $\vec{k}^{\prime\pm}$ are the momenta of the $n = 0$ magnons degenerate with the $n = 1$ magnons that are efficiently excited by the CoFeB Kittel mode when their \vec{k}^\pm is small. The amplitude of the $n = 1$ magnons therefore decreases with excitation frequency higher than $\approx 2 \min \omega_{1,\vec{k}}$, but $|\vec{k}^{\prime\pm}|$ of the $n = 0$ magnons increases. The secondary maximum of the spin pumping signals seen in experiments and calculations reveals that the four-magnon scattering can win this competition in a narrow frequency

interval. We do not observe indications for an intralayer three-magnon process in which one $n = 1$ YIG magnon splits into two $n = 0$ YIG magnons, because the overlap integrals are suppressed due to the different parity of the standing wave amplitudes (see SM, Sec. VI-B [47]). Finally, we demonstrate in Fig. 2(b) and SM Fig. S8 [47] excellent agreement of the calculated resonance energies with the observed spectra at both low and high excitation powers.

In conclusion, we detect nonlinear interlayer magnon interactions in a hybrid magnetic nanostructure (CoFeB|YIG) by nonlocal spin pumping. The leading nonlinearity is a three-magnon process in which one CoFeB Kittel magnon splits into a pair of single-node ($n = 1$) YIG magnons with opposite wave vectors ($+k$ and $-k$). By comparing the ISHE voltage signals on two Pt electrodes, we find nearly symmetric magnon emission to the left and right in contrast with the almost perfect chirality of linear excitations in agreement with model calculations based on purely magnetodipolar couplings. The theoretical analysis also indicates that the nonlinear interlayer coupling with single-node ($n = 1$) YIG magnons dominates over that with nodeless ($n = 0$) ones. We attribute an additional signal at even higher power to a cascade of *interlayer* three-magnon and *intralayer* four-magnon processes. Understanding the dynamics in hybrid magnetic systems may help engineer dissipation in nanomagnonic devices, which is a necessary step in the prospect of quantum magnonics for entanglement distillation through nonlinear coupling of local nanowire magnons and pairs of long-distance propagating magnons.

We thank R. Yuan and D. Wei for helpful discussions. The authors acknowledge support from the National Key Research and Development Program of China Grant No. 2022YFA1402801, and the NSF China under Grants No. 12074026, No. 12104208, and No. U1801661, and JSPS Kakenhi Grants No. JP19H00645 and No. 21K13847.

*These authors contributed equally to this work.

[†]haiming.yu@buaa.edu.cn

- [1] Th. Udem, R. Holzwarth, and T. W. Hänsch, Optical frequency metrology, *Nature (London)* **416**, 233 (2002).
- [2] Y. C. Mo, R. A. Kishek, D. Feldman, I. Haber, B. Beaudoin, P. G. O'Shea, and J. C. T. Thangaraj, Experimental Observations of Soliton Wave Trains in Electron Beams, *Phys. Rev. Lett.* **110**, 084802 (2013).
- [3] Z. Dutton, M. Budde, C. Slowe, and L. V. Hau, Observation of quantum shock waves created with ultra-compressed slow light pulses in a Bose-Einstein condensate, *Science* **293**, 663 (2001).
- [4] G. G. Rozenman, W. P. Schleich, L. Shemer, and A. Arie, Periodic Wave Trains in Nonlinear Media: Talbot Revivals, Akhmediev Breathers, and Asymmetry Breaking, *Phys. Rev. Lett.* **128**, 214101 (2022).
- [5] V. V. Kruglyak, S. O. Demokrotiv, and D. Grundler, Magnonics, *J. Phys. D* **43**, 264001 (2010).
- [6] A. V. Chumak, V. I. Vasyuchka, A. A. Serga, and B. Hillebrands, Magnon spintronics, *Nat. Phys.* **11**, 453 (2015).
- [7] V. Vlaminck and M. Bailleul, Current-induced spin-wave Doppler shift, *Science* **322**, 410 (2008).
- [8] L. J. Cornelissen, J. Liu, R. A. Duine, J. B. Youssef, and B. J. van Wees, Long-distance transport of magnon spin information in a magnetic insulator at room temperature, *Nat. Phys.* **11**, 1022 (2015).
- [9] P. Pirro, V. I. Vasyuchka, A. A. Serga, and B. Hillebrands, Advances in coherent magnonics, *Nat. Rev. Mater.* **6**, 1114 (2021).
- [10] A. Khitun, M. Bao, and K. L. Wang, Magnonic logic circuits, *J. Phys. D* **43**, 264005 (2010).
- [11] G. Csaba, A. Papp, and W. Porod, Perspectives of using spin waves for computing and signal processing, *Phys. Lett. A* **11**, 948 (2016).
- [12] Q. Wang *et al.*, A magnonic directional coupler for integrated magnonic half-adders, *Nat. Electron.* **3**, 765 (2020).
- [13] H. Suhl, The theory of ferromagnetic resonance at high signal powers, *J. Phys. Chem. Solids* **1**, 209 (1957).
- [14] S. M. Rezende and F. M. de Aguiar, Nonlinear dynamics in microwave driven coupled magnetic multilayer systems, *J. Appl. Phys.* **79**, 6309 (1996).
- [15] S. O. Demokritov, A. A. Serga, V. E. Demidov, B. Hillebrands, M. P. Kostylev, and B. A. Kalinikos, Experimental observation of symmetry-breaking nonlinear modes in an active ring, *Nature (London)* **426**, 159 (2003).
- [16] P. Krivosik and C. E. Patton, Hamiltonian formulation of nonlinear spin-wave dynamics: Theory and applications, *Phys. Rev. B* **82**, 184428 (2010).
- [17] P. A. Praveen Janantha, P. Sprenger, M. A. Hofer, and M. Wu, Observation of Self-Cavitating Envelope Dispersive Shock Waves in Yttrium Iron Garnet Thin Films, *Phys. Rev. Lett.* **119**, 024101 (2017).
- [18] C.-L. Ordóñez-Romero, B. A. Kalinikos, P. Krivosik, W. Tong, P. Kabos, and C. E. Patton, Three-magnon splitting and confluence processes for spin-wave excitations in yttrium iron garnet films: Wave vector selective Brillouin light scattering measurements and analysis, *Phys. Rev. B* **79**, 144428 (2009).
- [19] H. Kurebayashi, O. Dzyapko, V. E. Demidov, D. Fang, A. J. Ferguson, and S. O. Demokritov, Controlled enhancement of spin-current emission by three-magnon splitting, *Nat. Mater.* **10**, 660 (2011).
- [20] K. Ando and E. Saitoh, Spin Pumping Driven by Bistable Exchange Spin Waves, *Phys. Rev. Lett.* **109**, 026602 (2012).
- [21] H. J. Jason Liu, G. A. Riley, C. L. Ordóñez-Romero, B. A. Kalinikos, and K. S. Buchanan, Time-resolved study of nonlinear three-magnon processes in yttrium iron garnet films, *Phys. Rev. B* **99**, 024429 (2019).
- [22] H. Schultheiss *et al.*, Direct Current Control of Three Magnon Scattering Processes in Spin-Valve Nanocontacts, *Phys. Rev. Lett.* **103**, 157202 (2009).
- [23] R. E. Camley, Three-magnon processes in magnetic nano-elements: Quantization and localized mode effects, *Phys. Rev. B* **89**, 214402 (2014).
- [24] K. Schultheiss *et al.*, Excitation of Whispering Gallery Magnons in a Magnetic Vortex, *Phys. Rev. Lett.* **122**, 097202 (2019).

- [25] L. Körber, K. Schultheiss, T. Hula, R. Verba, J. Fassbender, A. Kákay, and H. Schultheiss, Nonlocal Stimulation of Three-Magnon Splitting in a Magnetic Vortex, *Phys. Rev. Lett.* **125**, 207203 (2020).
- [26] R. Verba, L. Körber, K. Schultheiss, H. Schultheiss, V. Tiberkevich, and A. Slavin, Theory of three-magnon interaction in a vortex-state magnetic nanodot, *Phys. Rev. B* **103**, 014413 (2021).
- [27] Z. Wang, H. Y. Yuan, Y. Cao, Z. X. Li, R. A. Duine, and P. Yan, Magnonic Frequency Comb through Nonlinear Magnon-Skyrmion Scattering, *Phys. Rev. Lett.* **127**, 037202 (2021).
- [28] C. Koerner, R. Dreyer, M. Wagener, N. Liebing, H. G. Bauer, and G. Woltersdorf, Frequency multiplication by collective nanoscale spin-wave dynamics, *Science* **375**, 1165 (2022).
- [29] I. Barsukov, H. K. Lee, A. A. Jara, Y.-J. Chen, A. M. Goncalves, C. Sha, J. A. Katine, R. E. Arisa, B. A. Ivanov, and I. N. Krivorotov, Giant nonlinear damping in nanoscale ferromagnets, *Sci. Adv.* **5**, eaav6943 (2019).
- [30] B. Divinskiy, S. Urazhdin, S. O. Demokritov, and V. E. Demidov, Controlled nonlinear magnetic damping in spin-Hall nano-devices, *Nat. Commun.* **10**, 5211 (2019).
- [31] M. Mohseni, Q. Wang, B. Heinz, M. Kewenig, M. Schneider, F. Kohl, B. Lägel, C. Dubs, A. V. Chumak, and P. Pirro, Controlling the Nonlinear Relaxation of Quantized Propagating Magnons in Nanodevices, *Phys. Rev. Lett.* **126**, 097202 (2021).
- [32] Y.-P. Wang, G.-Q. Zhang, D. Zhang, T.-F. Li, C.-M. Hu, and J. Q. You, Bistability of Cavity Magnon Polaritons, *Phys. Rev. Lett.* **120**, 057202 (2018).
- [33] M. Elyasi, Y.-M. Blanter, and G. E. W. Bauer, Resources of nonlinear cavity magnonics for quantum information, *Phys. Rev. B* **101**, 054402 (2020).
- [34] V. V. Konotop, J. Yang, and D. A. Zezyulin, Nonlinear waves in \mathcal{PT} -symmetric systems, *Rev. Mod. Phys.* **88**, 035002 (2016).
- [35] H. Jaeger and H. Haas, Harnessing nonlinearity: Predicting chaotic systems and saving energy in wireless communication, *Science* **304**, 78 (2004).
- [36] H. G. Craighead, Nanoelectromechanical systems, *Science* **290**, 1532 (2000).
- [37] P. Adhikari, M. Hafezi, and J. M. Taylor, Nonlinear Optics Quantum Computing with Circuit QED, *Phys. Rev. Lett.* **110**, 060503 (2013).
- [38] J. Li, S. Y. Zhu, and G. S. Agarwal, Magnon-Photon-Phonon Entanglement in Cavity Magnomechanics, *Phys. Rev. Lett.* **121**, 203601 (2018).
- [39] H. Y. Yuan, P. Yan, S. Zheng, Q. Y. He, K. Xia, and M. H. Yung, Steady Bell State Generation via Magnon-Photon Coupling, *Phys. Rev. Lett.* **124**, 053602 (2020).
- [40] D. Lachance-Quirion, S. P. Wolski, Y. Tabuchi, S. Kono, K. Usami, and Y. Nakamura, Entanglement-based single-shot detection of a single magnon with a superconducting qubit, *Science* **367**, 425 (2020).
- [41] S. Ecker, P. Sohr, L. Bulla, M. Huber, M. Bohmann, and R. Ursin, Experimental Single-Copy Entanglement Distillation, *Phys. Rev. Lett.* **127**, 040506 (2021).
- [42] V. Scarani, H. Bechmann-Pasquinucci, N. J. Cerf, M. Dusek, N. Lütkenhaus, and M. Peev, The security of practical quantum key distribution, *Rev. Mod. Phys.* **81**, 1301 (2009).
- [43] J. Ren *et al.*, Ground-to-satellite quantum teleportation, *Nature (London)* **549**, 70 (2017).
- [44] Y. Li, W. Zhang, V. Tyberkevych, W.-K. Kwok, A. Hoffmann, and V. Novosad, Hybrid magnonics: Physics, circuits, and applications for coherent information processing, *J. Appl. Phys.* **128**, 130902 (2020).
- [45] G. Gubbiotti, *Three-Dimensional Magnonics* (Jenny Stanford Publishing Pte. Ltd., Singapore, 2019).
- [46] F. Ciubotaru, T. Devolder, M. Manfrini, C. Adelmann, and I. P. Radu, All electrical propagating spin wave spectroscopy with broadband wavevector capability, *Appl. Phys. Lett.* **109**, 012403 (2016).
- [47] See Supplemental Material at <http://link.aps.org/supplemental/10.1103/PhysRevLett.130.046701> for sample preparation and SEM image of the CoFeB nanowire, microwave reflection spectra S_{11} measured by VNA on bare YIG and CoFeB|YIG samples, nonsaturated color map for the measurement at high power, anisotropy of the dispersion for the single-node mode, measurement on control samples with a nonmagnetic spacer, theory, spin pumping signals under different power at the right Pt electrode, single-node mode in a 40-nm-thick YIG film, measurement on a bare YIG control sample, measurement on a control sample with a 800-nm-wide CoFeB nanowire, and power-dependent measurements, which includes Refs. [48–52]
- [48] T. Wolfram and R. E. De Wames, Macroscopic and Microscopic Theories of Dipole-Exchange Spin Waves in Thin Films: Case of the Missing Surface States, *Phys. Rev. Lett.* **24**, 1489 (1970).
- [49] B. A. Kalinikos, M. P. Kostylev, N. V. Kozhus, and A. N. Slavin, The dipole-exchange spin wave spectrum for anisotropic ferromagnetic films with mixed exchange boundary conditions, *J. Phys. Condens. Matter* **2**, 9861 (1990).
- [50] A. Aharoni, Demagnetizing factors for rectangular ferromagnetic prisms, *J. Appl. Phys.* **83**, 3432 (1998).
- [51] L. R. Walker, Magnetostatic modes in ferromagnetic resonance, *Phys. Rev.* **105**, 390 (1957).
- [52] M. Elyasi, E. Saitoh, and G. E. W. Bauer, Stochasticity of the magnon parametron, *Phys. Rev. B* **105**, 054403 (2022).
- [53] Y. Tserkovnyak, A. Brataas, G. E. W. Bauer, and B. I. Halperin, Nonlocal magnetization dynamics in ferromagnetic heterostructures, *Rev. Mod. Phys.* **77**, 1375 (2005).
- [54] C. W. Sandweg, Y. Kajiwara, A. V. Chumak, A. A. Serga, V. I. Vasyuchka, M. B. Jungfleisch, E. Saitoh, and B. Hillebrands, Spin Pumping by Parametrically Excited Exchange Magnons, *Phys. Rev. Lett.* **106**, 216601 (2011).
- [55] O. d’Allivy Kelly *et al.*, Inverse spin Hall effect in nanometer-thick yttrium iron garnet/Pt system, *Appl. Phys. Lett.* **103**, 082408 (2013).
- [56] M. B. Jungfleisch, A. V. Chumak, A. Kehlberger, V. Lauer, D. H. Kim, M. C. Onbasli, C. A. Ross, M. Kläui, and B. Hillebrands, Thickness and power dependence of the spin-pumping effect in $Y_3Fe_5O_{12}/Pt$ heterostructures measured by the inverse spin Hall effect, *Phys. Rev. B* **91**, 134407 (2015).

- [57] Y. Cheng, A. J. Lee, G. Wu, D. V. Pelekhov, P. C. Hammel, and F. Yang, Nonlocal uniform-mode ferromagnetic resonance spin pumping, *Nano Lett.* **20**, 7257 (2020).
- [58] S. M. Rezende and F. M. de Aguiar, Spin-wave instabilities, auto-oscillations, and chaos in yttrium-iron-garnet, *Proc. IEEE* **78**, 893 (1990).
- [59] J. Chen, C. Liu, T. Liu, Y. Xiao, K. Xia, G. E. W. Bauer, M. Wu, and H. Yu, Strong Interlayer Magnon-Magnon Coupling in Magnetic Metal-Insulator Hybrid Nanostructures, *Phys. Rev. Lett.* **120**, 217202 (2018).
- [60] H. Schultheiss, K. Vogt, and B. Hillebrands, Direct observation of nonlinear four-magnon scattering in spin-wave microconduits, *Phys. Rev. B* **86**, 054414 (2012).
- [61] T. Hula, K. Schultheiss, A. Buzdakov, L. Körber, M. Bejarano, L. Flacke, L. Liensberger, M. Weiler, J. M. Shaw, H. T. Nembach, Jürgen Fassbender, and H. Schultheiss, Nonlinear losses in magnon transport due to four-magnon scattering, *Appl. Phys. Lett.* **117**, 042404 (2020).
- [62] J. Chen *et al.*, Excitation of unidirectional exchange spin waves by a nanoscale magnetic grating, *Phys. Rev. B* **100**, 104427 (2019).
- [63] T. Yu, Y. M. Blanter, and G. E. W. Bauer, Chiral Pumping of Spin Waves, *Phys. Rev. Lett.* **123**, 247202 (2019).
- [64] B. A. Kalinikos and A. N. Slavin, Theory of dipole-exchange spin wave spectrum for ferromagnetic films with mixed exchange boundary conditions, *J. Phys. C* **19**, 7013 (1986).
- [65] G. Dieterle, J. Forster, H. Stoll, A. S. Semisalova, S. Finizio, A. Gangwar *et al.*, Coherent Excitation of Heterosymmetric Spin Waves with Ultrashort Wavelengths, *Phys. Rev. Lett.* **122**, 117202 (2019).
- [66] M. Wu and A. Hoffmann, *Solid State Physics: Application of Microfocused Brillouin Light Scattering to the Study of Spin Waves in Low-Dimensional Magnetic Systems* (Academic Press, Burlington, VT, 2013), Vol. 63, p. 79–150.
- [67] D. D. Stancil and A. Prabhakar, *Spin Waves: Theory and Applications* (Springer, New York, 2009), Chap. 6, p. 191.
- [68] B. Pigeau, C. Hahn, G. de Loubens, V. V. Naletov, O. Klein, K. Mitsuzuka, D. Lacour, M. Hehn, S. Andrieu, and F. Montaigne, Measurement of the Dynamical Dipolar Coupling in a Pair of Magnetic Nanodisks Using a Ferromagnetic Resonance Force Microscope, *Phys. Rev. Lett.* **109**, 247602 (2012).
- [69] P. S. Keatley, P. Gangmei, M. Dvornik, R. J. Hicken, J. Grollier, and C. Ulysse, Isolating the Dynamic Dipolar Interaction between a Pair of Nanoscale Ferromagnetic Disks, *Phys. Rev. Lett.* **110**, 187202 (2013).
- [70] S. Klingler, V. Amin, S. Geprägs, K. Ganzhorn, H. Maier-Flaig, M. Althammer, H. Huebl, R. Gross, R. D. McMichael, M. D. Stiles, S. T. B. Goennenwein, and M. Weiler, Spin-Torque Excitation of Perpendicular Standing Spin Waves in Coupled YIG/Co Heterostructures, *Phys. Rev. Lett.* **120**, 127201 (2018).
- [71] H. Qin, S. J. Hämäläinen, and S. van Dijken, Exchange-torque-induced excitation of perpendicular standing spin waves in nanometer-thick YIG films, *Sci. Rep.* **8**, 5755 (2018).
- [72] Y. Li, W. Cao, V. P. Amin, Z. Zhang, J. Gibbons, J. Sklenar, J. Pearson, P. M. Haney, M. D. Stiles, W. E. Bailey, V. Novosad, A. Hoffmann, and W. Zhang, Coherent Spin Pumping in a Strongly Coupled Magnon-Magnon Hybrid System, *Phys. Rev. Lett.* **124**, 117202 (2020).
- [73] S. Emori, U. Bauer, S.-M. Ahn, E. Martinez, and G. S. D. Beach, Current-driven dynamics of chiral ferromagnetic domain walls, *Nat. Mater.* **12**, 611 (2013).
- [74] M. A. W. Schoen, D. Thonig, M. L. Schneider, T. J. Silva, H. T. Nembach, O. Eriksson, O. Karis, and J. M. Shaw, Ultra-low magnetic damping of a metallic ferromagnet, *Nat. Phys.* **12**, 839 (2016).
- [75] L. Flacke, L. Liensberger, M. Althammer, H. Huebl, S. Geprägs, K. Schultheiss, A. Buzdakov, T. Hula, H. Schultheiss, E. R. J. Edwards, H. T. Nembach, J. M. Shaw, R. Gross, and M. Weiler, High spin-wave propagation length consistent with low damping in a metallic ferromagnet, *Appl. Phys. Lett.* **115**, 122402 (2019).